Impurity modes in a two-dimensional photonic crystal: coupling efficiency and Q factor

Mario Agio, Elefterios Lidorikis, and Costas M. Soukoulis

Ames Laboratory and Department of Physics and Astronomy, Iowa State University, Ames, Iowa 50011

Received February 16, 2000; revised manuscript received July 14, 2000

A finite two-dimensional photonic crystal with a triangular lattice of air columns in a dielectric background is designed with a waveguide and a resonant cavity. By a time-domain solution of Maxwell's equations we observe the existence of impurity modes inside the photonic bandgap. An electromagnetic wave launched through the waveguide, with an appropriate frequency, can enhance the field inside the cavity and yield a peak in the transmission. Considering a manufactured structure, in which the columns are not perfectly equal, we repeat our calculations and analyze how the impurity modes are modified. For both cases, periodic and real, we measure the quality factor of the cavity. © 2000 Optical Society of America [S0740-3224(00)01012-2]

OCIS codes: 230.7370, 230.5750.

1. INTRODUCTION

In recent years it has been proposed that a structure with a periodic dielectric constant, named a photonic crystal (PC), can affect the transmission of light and the photonic density of states.[1,2] This property is due to the existence of the photonic bandgap (PBG), a range of frequencies in which the propagation of the electromagnetic field is forbidden. In fact, the dielectric constant acts as a periodic scatterer, which, in analogy with the potential felt by an electron in a crystal, modifies the dispersion relation of light and builds photonic bands and PBG's. Furthermore, the insertion of defects in PC's creates localized modes inside the PBG.[3–13] Localization depends on different factors: the periodicity of the dielectric constant, the defect itself, and the PBG. Considering a two-dimensional (2D) PC, that is, with the dielectric constant periodic in a plane and homogeneous in the direction normal to that plane, for in-plane propagation, a line defect represents a waveguide (WG), and a point defect is a resonant cavity (RC). Theoretical as well as experimental investigations have demonstrated the efficiency of 2D PC's as WG's or RC's. Because of the scaling properties of PC's,[3] the stated performances remain valid for every frequency. These features are fundamental in designing optical circuits and other photonic devices when light has to be driven through sharp bends. However, the fact that PC's must be artificially manufactured constitutes a technological challenge, in particular if the PC requires a micrometer lattice constant to operate at infrared and higher frequencies.[14–17]

It is interesting to extend the analysis to more complicated configurations with WG's and RC's. In this report we theoretically study a 2D PC with a WG and a RC that has been fabricated in Halle for the mid-infrared region.[16,18] The structure, a triangular lattice of air columns in a silicon background, has some missing columns that build a WG interrupted in the middle by a RC; see Fig. 1 and the respective caption for details. The lattice constant, a, is 1.5 μm, and the column's diameter, d, is 1.28 μm. We consider both an ideal PC, where every column has exactly the same radius, and the real PC with columns not perfectly equal. With a finite-difference time-domain technique we seek impurity modes inside the PBG and measure the quality (Q) factor[19] of the cavity. Monochromatic light, polarized with the magnetic field along the column's axis, propagates through the WG and reaches the RC. The WG is designed to facilitate the coupling between the incident field and the RC and to drive the radiation emitted by the impurity mode.

We measure the transmission at the opposite side of the PC. For certain wavelengths a cavity mode is excited. This is represented by a narrow peak in the transmission: electromagnetic energy is temporarily stored in the cavity, and then it is released in every direction, but, since the wavelength is in the PBG, it is guided through the WG. We find four impurity modes for the ideal structure and four impurity modes for the real one. For each peak a snapshot of the field inside the cavity at the steady state proves that energy is really stored and that the field corresponds to a cavity mode, with a specific pattern. We investigate the differences in the peaks and in the field patterns between ideal and real PC's. Finally, we measure the Q factor by quenching the source and calculating the rate of decay of the energy stored in the RC.

In Section 2 we explain the numerical method used to solve Maxwell's equation, including measurements of the transmission's coefficient and the Q factor; in Section 3 we show and discuss the numerical results for the ideal and the real PC, with field analysis and the Q factor; in Section 4 we briefly sum up our results.

2. METHOD

To inspect the existence of impurity modes and to evaluate the Q factor of the cavity, we solve Maxwell's equations in the time-domain regime. To simplify the problem, we assume that the dielectric medium is lossless, and we fix the magnetic permeability to 1. Furthermore, since our PC is infinitely extended along the column's

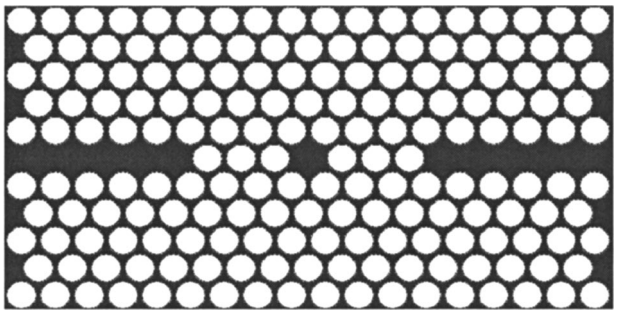

Fig. 1. Two-dimensional photonic crystal with a triangular lattice. The missing columns yield a waveguide and a resonant cavity in the middle. There are 18×11 unit cells with lattice constant $a = 1.5\,\mu$m; air columns have diameter $d = 1.28\,\mu$m. The dielectric background is silicon, $\epsilon_d = 11.9$. The source is put at the left side of the structure, in front of the WG.

axis, for in-plane propagation the electromagnetic field is decoupled in TE (TM) modes, when the magnetic (electric) field is parallel to the columns. Thus the fields are governed by the following equations:

$$\frac{\partial}{\partial t}\mathbf{H}(\mathbf{r}, t) = -\nabla \times \mathbf{E}(\mathbf{r}, t), \tag{1}$$

$$\epsilon(\mathbf{r})\frac{\partial}{\partial t}\mathbf{E}(\mathbf{r}, t) = \nabla \times \mathbf{H}(\mathbf{r}, t), \tag{2}$$

where $\epsilon(\mathbf{r})$ is the modulated dielectric constant. We tackle Eqs. (1) and (2) with a finite-difference time-domain technique.[20] The real space is discretized in a fine square grid that stores the dielectric constant and the fields' values. Since it is not possible to extend the storage to the whole space, we truncate the grid as soon as it compasses the PC. By use of a finite time step the fields are recursively updated on every grid point. At the edges, to avoid backreflection, the fields are updated with Liao boundary conditions.[21] This algorithm[22] numerically reproduces the propagation of the electromagnetic field in real space and time through the PC. In our calculations we used a grid with a pitch of 50 nm, which is 1/30 of the lattice constant.

The radiating source is a TE monochromatic wave, with a Gaussian amplitude along the direction orthogonal to the WG, and is located at the left side of the PC, in front of the WG. Having chosen a wavelength, we look for a steady-state solution to excite possible impurity modes. We measure the Poynting vector and the amplitude of the electric field at the beginning and at the end of the WG. To obtain reliable results, we averaged these values on a small spot of the grid and in time, too. Then, transmission is given by scaling the square of the transmitted electric field with the square of the incident electric field, or equally, by the ratio of the outgoing and the incident Poynting vectors. We did both just to test our data. We examine a wavelength range that goes from 3 to 6 μm, a region in which our structure exhibits a PBG.

In correspondence to an impurity mode we calculate the field's patterns to understand how the symmetry of the RC affects the field's distribution. Besides, we evaluate the storage of electromagnetic energy inside the RC; the source pumps energy in the RC. Having reached the steady state, the source is switched off and the energy begins to decay exponentially. The decay's rate is given by

$$\frac{dE}{dt} = -\frac{2\pi c}{\lambda_0 Q}E, \tag{3}$$

where λ_0 is the resonant wavelength, c is the speed of light, and Q is the quality factor. Thus calculating the energy's storage and its decay rate, from Eq. (3) we draw the Q factor of the RC. The Q factor is also given by $\omega_0/\Delta\omega$, where ω_0 is the resonant frequency and $\Delta\omega$ is the bandwidth at the half-height of the Lorentzian peak. However, we choose the former method because it is more accurate.

3. RESULTS

We consider a 2D PC with a triangular lattice of air columns in silicon ($\epsilon_d = 11.9$). The structure is made of 18×11 unit cells, with lattice constant $a = 1.5\,\mu$m. The column's diameter is $d = 1.28\,\mu$m. As depicted in Fig. 1, in the middle of the sample, some missing columns model a WG and a RC. We carry out our calculations on an ideal structure (see Fig. 1) and on a real structure, manufactured at Halle[18] (see Fig. 2). In Fig. 2 the numbers in the air holes represent the real diameter expressed in micrometers. These labeled holes have an average diameter equal to 1.23 μm. For the other holes we assume the diameter of the ideal structure ($d = 1.28\,\mu$m).[23] In the following subsections we compare the results obtained from the two structures, ideal and real.

A. Transmission

In Fig. 3 we plot the transmission for both the ideal and the real PC's. The solid curve refers to the ideal case, and the dashed curve refers to the real one. A PBG occurs for λ between 3.4 and 5.5 μm, as regards the ideal structure, and for λ between 3.5 and 5.6 μm, as regards the real structure. The PBG is featured by a drop in the transmission of more than six orders of magnitude. This means that despite the presence of the WG, the six columns that shape the RC are enough to completely stop

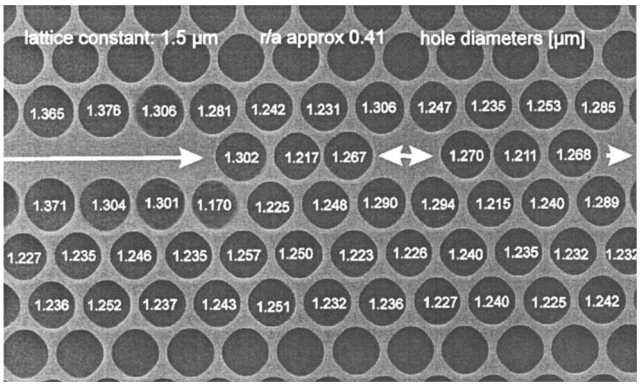

Fig. 2. SEM picture of the sample manufactured at Halle. The numbers inside the holes represent the real diameter in micrometers. The average diameter of the marked holes is $d_{av} = 1.23\,\mu$m. For the other holes we chose $d = 1.28\,\mu$m, as it is in the ideal structure. The depth of column etching is 100 μm.

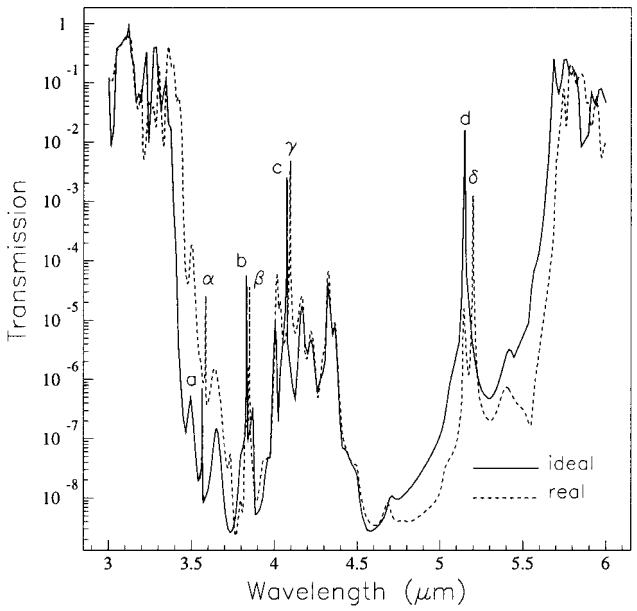

Fig. 3. Transmission for λ between 3.0 and 6.0 μm. The solid (dashed) curve refers to the ideal (real) structure. Each impurity mode is marked with an italic (Greek) letter for the ideal (real) case. The corresponding wavelengths are a (3.564 μm), b (3.830 μm), c (4.074 μm), d (5.147 μm), α (3.585 μm), β (3.848 μm), γ (4.095 μm), and δ (5.198 μm).

the propagation of the electromagnetic field toward the other side of the WG. At the same time, inside the PBG, these columns are able to trap the field in the center of the structure, inside the RC. Thus when a wave routes the WG, the issue is if the incident field couples with a cavity mode. If coupling occurs, it excites a particular mode depending on the wavelength of the source. Since the resonant field radiates in every direction, the WG captures the outgoing power and drives it to the right end of the PC. This effect increases the transmission orders of magnitude. Indeed, spanning the PBG by varying the wavelength of the source, we find some peaks: four for the ideal structure and four for the other one. For the first case the resonant peaks are marked with italic letters and occur at these wavelengths: 3.564, 3.830, 4.074, and 5.147 μm. For the second case they are marked with Greek letters and occur for λ equal to 3.585, 3.848, 4.095, and 5.198 μm.

To better understand the role of the WG, we calculate the transmission for the same structure, but by completely removing the central row of air cylinders, i.e., without the RC. In this case we get information on how much power is driven through the WG itself. For $\lambda \simeq 3.920\ \mu$m there is a dip in the transmission, but for the other wavelengths inside the PBG the transmission is almost 100%. In Fig. 3 the peaks are positioned where the WG transmits well and, for $\lambda \simeq 3.920\ \mu$m, the drop is orders of magnitudes larger than the corresponding dip for the WG. Therefore we argue that, for this structure, the WG provides a good feeding for the cavity modes and that the drop in Fig. 3 derives primarily from the presence of the six cylinders in the central row.

The transmission peaks are sharp and well separated, in accordance with the fact that they belong to the discrete spectrum of a microcavity. Comparing the two structures, we notice that the peaks of the real PC have a redshift. The reason relies on the size of the RC. In fact, a larger cavity can sustain modes with a lower frequency. As a rule of thumb, since for the real case the columns around the RC are smaller on average ($d_{av} = 1.23\ \mu$m) than for the ideal case, the dielectric region left at the center is larger and increases the size of the RC. This yields the redshift in the resonances.

Since the impurity mode is inside the PBG, the electric field is localized in the RC. The excitation of these modes and the transmission is performed by the WG, which conveys electromagnetic energy inward to and outward from the RC. The inspection of the electric field's pattern offers a further insight on the coupling efficiency.

B. Field's Analysis

When an impurity mode is excited, the field is in resonance with the microcavity. The more the electromagnetic field is enhanced, the larger the transmission is. The peaks in Fig. 3 have different heights; that is, some of them are more easily excited than others. The coupling efficiency stems from several parameters, such as the wavelength of the source and the presence of PBG's and defects (WG and RC). In our investigation we vary only the incident wavelength.

Figure 4 shows snapshots of the normalized electric field for the four peaks regarding the ideal structure. When the source is tuned on a resonant wavelength, it excites a particular impurity mode. As an example, for $\lambda = 3.564\ \mu$m the field is a hexapole, which resembles the whispering-gallery mode observed in microdisk lasers' cavities. We notice that the shape of the cavity is fundamental for the field's pattern. In fact, a RC made with a

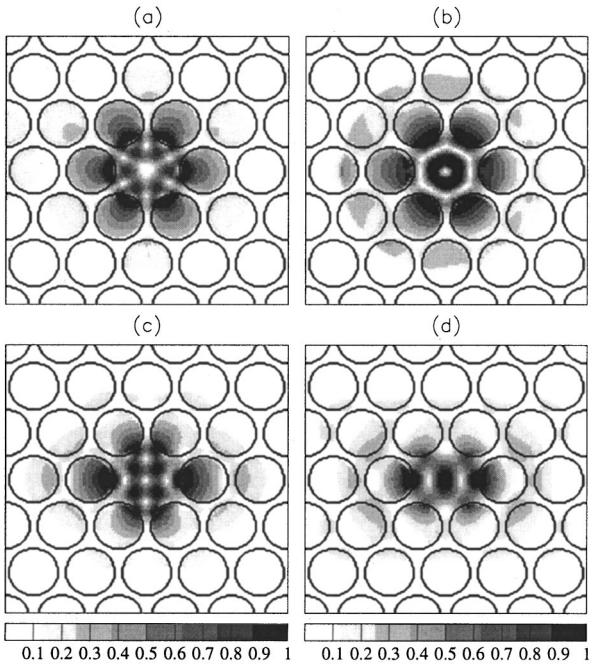

Fig. 4. Normalized amplitude of the electric field for the impurity modes of the ideal structure: (a) hexapole $\lambda = 3.564\ \mu$m, (b) monopole $\lambda = 3.830\ \mu$m, (c) decapole $\lambda = 4.074\ \mu$m, and (d) so-called pentapole $\lambda = 5.147\ \mu$m.

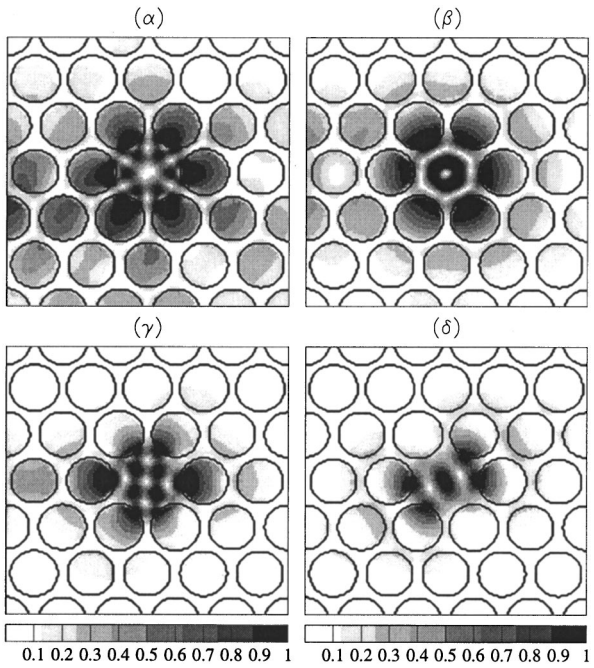

Fig. 5. Normalized amplitude of the electric field for the impurity modes of the real structure: (α) hexapole $\lambda = 3.585\ \mu$m, (β) monopole $\lambda = 3.848\ \mu$m, (γ) decapole $\lambda = 4.095\ \mu$m, and (δ) pentapole $\lambda = 5.198\ \mu$m.

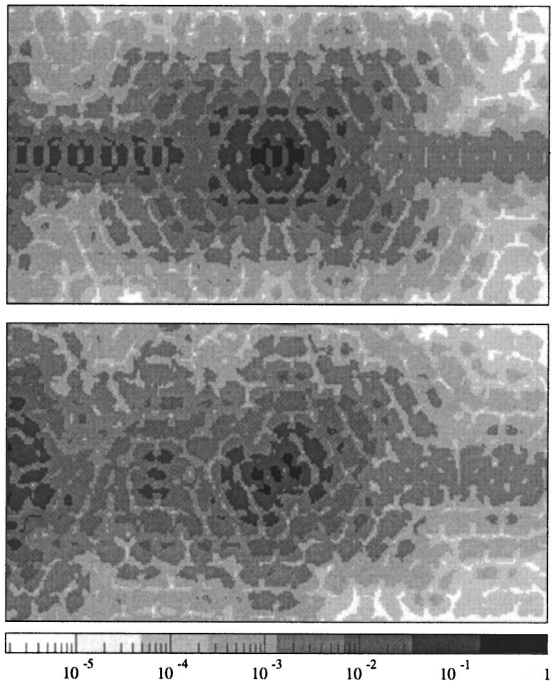

Fig. 6. Normalized amplitude of the electric field for the modes (d) $\lambda = 5.147\ \mu$m (top panel) and (δ) $\lambda = 5.198\ \mu$m (bottom panel). The snapshots, which are contour plots in log scale, cover the whole structure.

square lattice instead of a triangular one shall sustain different modes.[7,9] The field's distribution of the decapole [Fig. 4(c)] and the so-called pentapole [Fig. 4(d)] is toward the WG, and for the hexapole and the monopole the field has a sixfold symmetry. Thus the former modes favor the coupling between the WG and the RC. On the contrary, a mode with sixfold symmetry directs energy toward the six symmetry directions with the same intensity. Now it is clear why the peaks at 4.074 and 5.147 μm give a larger transmission than the other peaks do; see Fig. 3. Definitively, the coupling efficiency is strongly correlated to the impurity mode excited in the RC.

Another important issue to consider is the difference between ideal and real PC's. The height of the peaks in the real case is smaller than that of the ideal case. This suggests that an irregularity in the structure degrades the RC and the coupling efficiency. In fact, as shown in Fig. 2, variations in the holes' diameters break the sixfold symmetry of the RC, in particular because of the mismatch 1.306 μm versus the nearest cylinders. Figure 5 is the correspondent of Fig. 4 for the real structure. The modes are classified by use of the same nomenclature: (α) hexapole, (β) monopole, (γ) decapole, and (δ) pentapole. Comparing the pentapole mode with the same one in the ideal case, we observe that the intensity is not so well oriented toward the WG as previously. The difference among the pentapole patterns is shown in Fig. 6, where the snapshots are extended to the whole structure. We notice also that the secondary lobes of the cavity modes are rotated with respect the WG. This feature stems mainly from the mismatches 1.306 μm versus nearest columns, or primary lobes, and 1.302 μm again versus nearest columns, or secondary lobes. Consequently, the coupling decreases and the transmission is lower, as is shown in Fig. 3 for the peaks around $\lambda = 5.1\ \mu$m. For the other modes the coupling efficiency is not much degraded, since the patterns are almost unchanged, also as regards the secondary lobes. Indeed, the transmission peaks have a comparable height. However, the large difference between a and α is due to the shift of the gap's edge, but the relative heights are more or less equal.

The study of the impurity modes shows the tight correlation between coupling and field distribution. This gives the reason of the peaks' heights, but not of their widths, since the broadening of a peak is related to the Q factor.

C. Quality Factor

The Q factor is an estimate of the capability to sustain free cavity modes lasting in time. In this subsection we evaluate the Q factor for each cavity mode found in the ideal and real structures.

Using the technique discussed in Section 2, we calculate the amount of energy inside the RC as a function of time, when the source is turned off.[24] Plotting the results in a linear-log scale, we find that the rate of the energy's decay is exponential, as predicted by Eq. (3). The values of the Q factors, calculated for every peak and for both ideal and real cases, are shown in Table 1. We note that the Q factor is not constant when the wavelength is varied. In fact, the peaks are spectrally scattered within the PBG. As a consequence, the field's attenuation can be different at different frequencies within the PBG. The peak α has the lowest Q factor since it is very close to the PBG's edge. This does not happen for peak a because the edge is shifted and the transmission has already dropped.

Table 1. Quality Factor for the Impurity Modes

Case	Q Factor[a]			
Ideal	a	b	c	d
	27000	18500	37500	11300
Real	α	β	γ	δ
	7500	12500	20600	29700

[a] The Greek and italic letters mark the peaks as assumed in Fig. 3.

There is a large difference between the Q factors of the d peak and of the δ peak. Moreover, in this case only, the real structure exhibits a higher Q factor than the ideal one. Referring to Fig. 6, we argue that the small overlap between the WG and the intensity's lobes of the electric field degrades the coupling efficiency. Therefore the losses through the WG are reduced, and, consequently, the mode of the real structure gains a higher Q factor.

In general for both ideal and real structures, the Q factor is very high, $> 10^4$. Despite only three columns separating the WG from the RC, the energy storage is very effective, and the power radiated by the resonant modes is collected and guided by the WG.

4. CONCLUSIONS

We investigate the coupling between a WG and a RC designed in a 2D PC with triangular lattice. By use of a source, harmonic waves are launched through the WG, which conveys electromagnetic power toward the RC. When a cavity mode is excited inside the PBG, a transmission peak occurs. By a field analysis of the four peaks, we find a connection between coupling efficiency and mode patterns. A strong coupling gives a large increase in transmission. We calculate high Q factors, despite the RC having only three columns per part along the WG. The Q factor is different for each cavity mode, depending on the peak's position inside the PBG. We also consider two structures, ideal and real. They give almost the same results, but a comparison shows how irregularities may affect the coupling efficiency and the Q factor. In conclusion, a WG is useful to force oscillations in a RC because at the same time it carries and drains power, improving the performances of the RC.

The next step is to better understand how to tune the impurity modes by changing parameters such as the dielectric contrast, the columns' radii, and the lattice itself. To find the optimized structure it would also be interesting to add or remove the columns that connect the WG to the RC. Then, to be more realistic, it would be worth taking into account the finite height of the columns to know how much energy is lost by diffraction and if this degrades the Q factor.

ACKNOWLEDGMENTS

Ames Laboratory is operated for the U.S. Department of Energy by Iowa State University under Contract W-7405-Eng-82. This research was also supported by a PCIC European Union grant. This research was supported by the director for Energy Research, office of Basic Energy Sciences.

REFERENCES AND NOTES

1. E. Yablonovich, "Inhibited spontaneous emission in solid-state physics and electronics," Phys. Rev. Lett. **58**, 2059–2062 (1987).
2. S. John, "Strong localization of photons in certain disordered dielectric superlattices," Phys. Rev. Lett. **58**, 2486–2489 (1987).
3. J. D. Joannopoulos, R. D. Meade, and J. N. Winn, *Photonic Crystals—Molding the Flow of Light* (Princeton University, Princeton, N.J., 1995).
4. C. M. Soukoulis, ed., *Photonic Band Gaps Materials*, Vol. 315 of NATO ASI Ser., Ser. E Applied Sciences (Kluwer Academic, Dortrecht, The Netherlands, 1996).
5. C. Weisbuch and J. Rarity, eds., *Microcavities and Photonic Band Gaps: Physics and Applications*, Vol. 324 of NATO ASI Ser., Ser. E Applied Sciences (Kluwer Academic, Dortrecht, The Netherlands, 1996).
6. R. D. Meade, A. Devenyi, J. D. Joannopoulos, O. L. Alerhand, D. A. Smith, and K. Kash, "Novel applications of photonic band gap materials: low-loss bends and high Q cavities," J. Appl. Phys. **75**, 4753–4755 (1994).
7. P. R. Villeneuve, S. Fan, and J. D. Joannopoulos, "Microcavities in photonic crystals: mode symmetry, tunability, and coupling efficiency," Phys. Rev. B **54**, 7837–7842 (1996).
8. A. Mekis, J. C. Chen, I. Kurland, S. Fan, P. R. Villeneuve, and J. D. Joannopoulos, "High transmission through sharp bends in photonic crystal waveguides," Phys. Rev. Lett. **77**, 3787–3790 (1996).
9. J. D. Joannopoulos, P. R. Villeneuve, and S. Fan, "Photonic crystals: putting a new twist on light," Nature **386**, 143–149 (1997).
10. J. S. Foresi, P. R. Villeneuve, J. Ferrera, E. R. Thoen, G. Steinmeyer, S. Fan, J. D. Joannopoulos, L. C. Kimerling, H. I. Smith, and E. P. Ippen, "Photonic-bandgap microcavities in optical waveguides," Nature **390**, 143–145 (1997).
11. S.-Y. Lin, E. Chow, V. Hietala, P. R. Villeneuve, and J. D. Joannopoulos, "Experimental demonstration of guiding and bending of electromagnetic waves in a photonic crystal," Science **282**, 274–276 (1998).
12. B. D'Urso, O. Painter, J. O'Brien, T. Tombrello, A. Yariv, and A. Scherer, "Modal reflectivity in finite-depth two-dimensional photonic-crystal microcavities," J. Opt. Soc. Am. B **15**, 1155–1159 (1998).
13. H. Benisty, C. Weisbuch, D. Labilloy, M. Rattier, C. J. M. Smith, T. F. Krauss, R. M. De La Rue, R. Houdré, U. Oesterle, C. Jouanin, and D. Cassagne, "Optical and confinement properties of two-dimensional photonic crystals," J. Lightwave Technol. **17**, 2063–2077 (1999).
14. T. F. Krauss, R. M. De La Rue, and S. Brand, "Two-dimensional photonic-bandgap structures operating at near-infrared wavelengths," Nature **383**, 699–701 (1996).
15. D. Labilloy, H. Benisty, C. Weisbuch, T. F. Krauss, R. M. De La Rue, V. Bardinal, R. Houdré, U. Oesterle, D. Cassagne, and C. Jouanin, "Quantitative measurement of transmission, reflection, and diffraction of two-dimensional photonic band gap structures at near-infrared wavelengths," Phys. Rev. Lett. **79**, 4147–4150 (1997).
16. A. Birner, U. Grüning, S. Ottow, A. Schneider, F. Müller, V. Lehmann, H. Föll, and U. Gösele, "Macroporous silicon: a two-dimensional photonic bandgap material suitable for the near-infrared spectral range," Phys. Status Solidi A **165**, 111–117 (1998).
17. D. Labilloy, H. Benisty, C. Weisbuch, C. J. M. Smith, T. F. Krauss, R. Houdré, and U. Oesterle, "Finely resolved transmission spectra and band structure of two-dimensional pho-

tonic crystals using emission from InAs quantum dots," Phys. Rev. B **59**, 1649–1652 (1999).
18. A. Birner, Max-Planck-Institüt, Halle, Germany (private communication, 2000).
19. J. D. Jackson, *Classical Electrodynamics* (Wiley, New York, 1975).
20. A. Tavlove, *Computational Electrodynamics—The Finite-Difference Time-Domain Method* (Artech House, Norwood, Mass., 1995).
21. Z. P. Liao, H. L. Wong, B. P. Yang, and Y. F. Yuan, "A transmitting boundary for transient wave analyses," Sci. Sinica A **27**, 1063–1076 (1984).
22. K. S. Yee, "Numerical solution of initial boundary value problems involving Maxwell's equations in isotropic media," IEEE Trans. Antennas Propag. **AP-14**, 302–307 (1966).
23. The four digits diameters' values, shown in Fig. 2, are determined by the Halle group from the analysis of the SEM picture. Because of the fluctuations along the pores and the method used to obtain the diameters, only the first three digits are reliable. However, the fourth digit does not significantly affect the results and can be neglected in the calculations.
24. When the source is suddenly switched off, all frequencies are introduced. However, they rapidly fade away, and the frequency of the cavity mode is the only one surviving.